The Hadronic Final State at HERA

Rainer Mankel

DESY, Notkestr 85, D-22603 Hamburg, Germany

for the H1 and ZEUS collaborations

Received Nov 30, 2005

The electron-proton collider HERA offers unique capabilities to study the properties of the hadronic final state. This paper summarizes selected results highlights from the colliding beam experiments H1 and ZEUS.

PACS: 13.60.-r, 13.60.Rj
Key words: leading proton, leading neutron, forward jet, rapidity gap, beauty production

1 Introduction

Observation of ep collisions at HERA provides an excellent window to study the hadronic final state. This becomes evident when comparing the final state topology of ep collisions to other interaction types: in e^+e^- collisions, the hadronic final state consists frequently of two quark jets and can be measured cleanly, but lacks the element of a proton remnant which would be important to describe hadronic interactions relevant for cosmic ray physics. Proton-proton interactions on the other hand are very complex to measure and understand, because of the hadronization of the second proton. In this comparison, the final state of the ep collision represents the golden way in between, since it features the main elements of quark and proton remnant fragmentation, but is at the same time free of the additional complication of a second baryonic system.

There is a marked difference between collider experiments and the way interactions present themselves in cosmic ray studies. As visible in fig.1 [1], collider experiments have excellent access to the scattered lepton in case of a neutral current (NC) interaction, and to the fragmentation products of the scattered quark, the current jet. The debris of the proton remnant, however, appear in the vicinity of the beam pipe and are generally less accessible. In cosmic ray experiments, there is no such distinction, and it is essential that theoretical models are tuned such that they describe the proton remnant region equally well.

One of the main questions addressed in this article is therefore how well we currently understand the workings of QCD in the forward area. In addition, the rôle of the diffractive component at high energies, and the measurement of the production of heavy flavors and the resulting leptons will be addressed.

2 Production of Leading Baryons

A sizable fraction of ep collisions contains leading baryons, and their measurement provides an excellent way of improving the understanding of hadronization in the proton remnant area. At HERA, precision measurements of leading protons and neutrons are obtained with special forward detectors, which are named FPS (Forward Proton Spectrometer) and FNC (Forward Neutron Calorimeter) in the case of H1, and LPS (Leading Proton Spectrometer) and FNC at ZEUS. The LPS, for example, consists of six stations of roman pots in the curve of the proton beam downstream of the ZEUS main detector, surrounded by HERA dipole and quadrupole magnets. Each station is equipped with six silicon detector planes. The fractional energy of the outgoing leading proton, $x_L = E_{LP}/E_p$ can be measured in the range $0.4 < x_L < 1$, its transverse momentum p_T in the region $p_T^2 < 0.5\ GeV^2$.

Mainly two mechanisms are expected to contribute to leading baryon production. It is straightforward to assume that leading protons are produced by hadronisation of the proton remnant, as addressed by standard fragmentation models. Such models predict for $x_L > 0.4$ a marked decrease of the cross section with a moderate power of $(1 - x_L)$ [2]. An alternative theoretical approach is based on the exchange of a virtual particle between the incident proton and a hadronic system into which the virtual photon has dissociated; this virtual particle might typically be a π^0, pomeron or Reggeon in the case of leading proton production, and a π^+ (or ρ^+) in case of leading neutrons.

The x_L spectrum has been measured with very good precision (fig.2) [3] and reveils an entirely different shape than would be expected from proton remnant

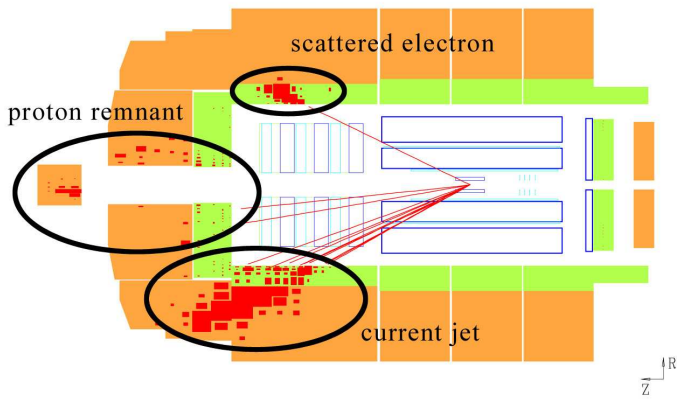

Fig. 1. Display of a DIS event measured with the H1 detector.

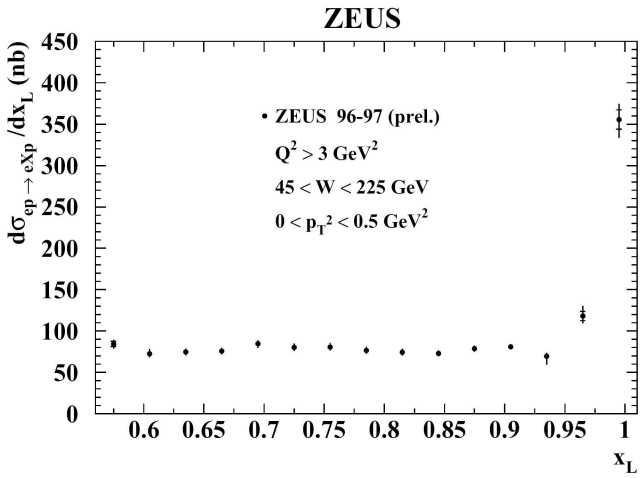

Fig. 2. Differential cross section $d\sigma(ep \to eXp)/dx_L$ in the kinematic range $x_L > 0.56$, $p_T^2 < 0.5\ GeV^2$, $Q^2 > 3\ GeV^2$ and $45 < W < 225\ GeV$.

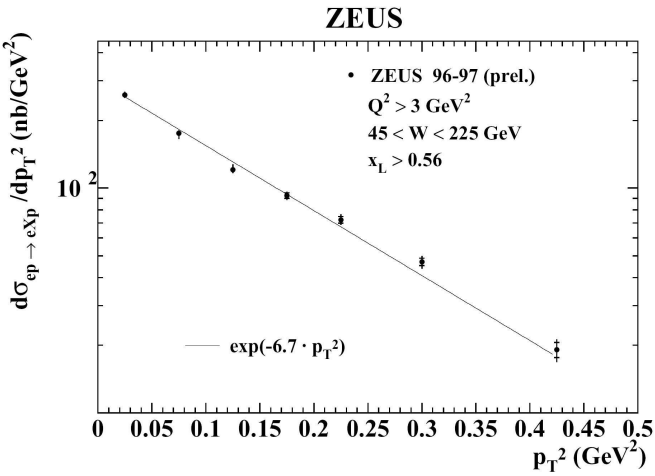

Fig. 3. Differential cross section $d\sigma(ep \to eXp)/dp_T^2$ in the kinematic range of fig. 2.

fragmentation: apart from the diffractive peak near $x_L \sim 1$, the cross section is essentially constant between 0.6 and 0.9. The transverse shape (fig. 3) can be described well by a parametrization of the form $d\sigma/dp_T^2 \propto exp(-b(x_L)\ p_T^2)$, with the slope parameter b not strongly dependent on x_L, once more a behavior not described by models of proton remnant fragmentation [2].

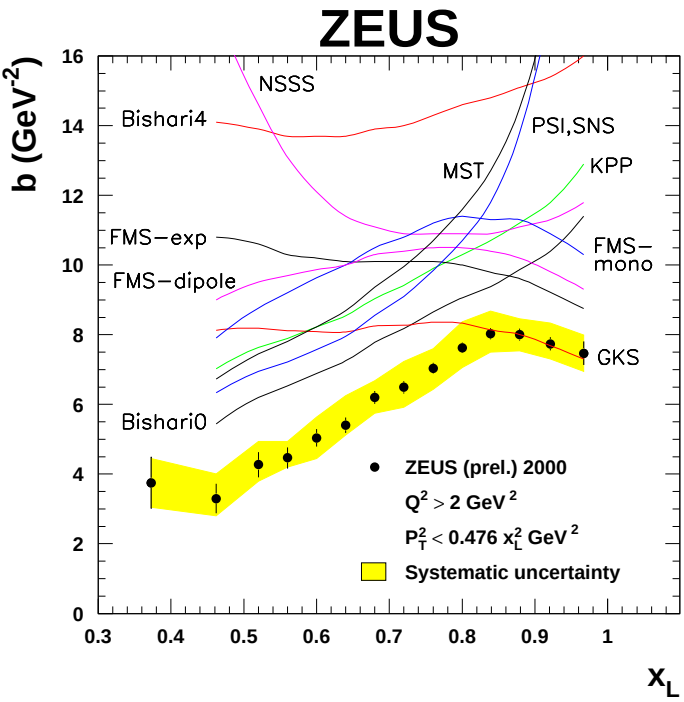

Fig. 4. Transverse slope parameter b from exponential fits of the p_T^2 distributions as a function of x_L for leading neutron production. Predictions of various models of one-pion exchange are also shown as curves (see references in [4]).

In view of this unexpected behavior, it is very instructive to examine the production of leading neutrons for comparison. The measured dependence of the transverse momentum slope parameter, $b(x_L)$ is displayed in fig. 4 [4]. The steepness of the p_T spectra is strongly increasing with x_L, which points to different underlying dynamics in this process. In the case of leading neutrons, the situation for investigation of virtual partical exchange is very favorable, since exchange of one particle (π^+) is expected to dominate.

Particle exchange models factorize the cross section into one factor describing the pion flux from the proton, and the pion-photon cross section in the form

$$\frac{d\sigma_{ep\to eXn}(W^2, Q^2, x_L, t)}{dx_L dt} = f_\pi(x_L, t) \cdot \sigma_{\gamma^*\pi}((1-x_L)W^2, Q^2)$$

The high precision of the data allows for very accurate comparisons with various models as displayed in fig. 4. It is possible to constrain parameters on some models, and to exclude other models. Some model predictions come rather close to achieving a good description of the data.

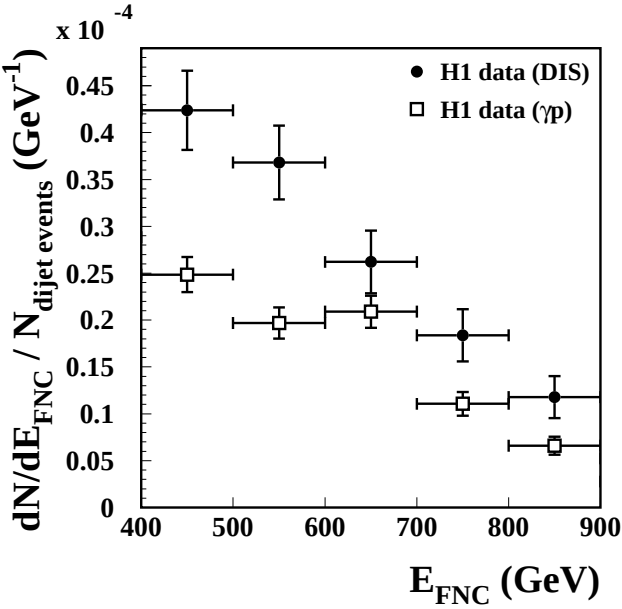

Fig. 5. Energy distributions observed in the H1 FNC for di-jet events in photoproduction and DIS data, normalized to the respective number of di-jet events in each inclusive di-jet sample.

More detailed comparisons are possible by investigating events in which the leading neutron is accompanied by two jets. Also in this subsample, pion exchange models are found to describe the data quite well [5]. The fraction of leading neutrons is significantly higher in DIS di-jet events than in photo-production di-jet events (fig. 5), where the difference is most pronounced at lower neutron energies.

3 Forward Jets

The forward area is particularly sensitive to details in the evolution of the parton cascade. The variable $x \equiv x_{Bj}$ is normally interpreted as the fraction of proton momentum that the quark struck by the virtual photon was carrying. At low values of x, however, where the interaction is mediated by a parton cascade (fig. 6 [6]), we no longer probe the valence structure of the proton, but rather see the

universal structure of QCD radiation at work. At small x, a sizeable fraction of the proton momentum can manifest itself in an energetic forward jet, which provides an excellent signature to probe the mechanisms of parton cascade evolutions.

Describing the dynamics of parton evolution is the target of essentially three different approaches: the DGLAP evolution [7] is performed in powers of $\ln Q^2$ and leads to a strong ordering in k_T. This approach is well established at high x and Q^2, but expected to break down at low x. The BFKL evolution [7] is performed in powers of $\ln 1/x$ and results in a strong ordering in x. The CCFM evolution [7], which aims to combine the virtues of DGLAP and BFKL, is performed in both $\ln Q^2$ and $\ln 1/x$ and leads to an angular ordering. Both BFKL and CCFM evolution may be applicable at low x.

Events with forward jets have been selected such that the effects of BFKL-style evolutions are expected to show ($x_{Bj} < 0.004$, $7^\circ < \theta_{jet} < 20^\circ$, $x_{jet} > 0.035$) [6]. Figure 7 shows the measured differential cross section in x_{Bj} in comparison to theoretical models. The model with DGLAP evolution (DISENT) underestimates the data by a factor of 2 at low x even at NLO level. Also the CCFM model (CASCADE) predicts a distribution which is too hard. The BFKL-inspired color dipole model however gives a generally good description of the data. Limitations of the pure DGLAP approach are also seen in a subsample with an additional di-jet signature [6].

4 Diffractive Final States at High Q^2

Diffractive processes are a significant component of the total DIS cross section. For a thorough understanding of the hadronic final state, it is an interesting question how far such processes extend into the high Q^2 regime. Diffractive exchange is

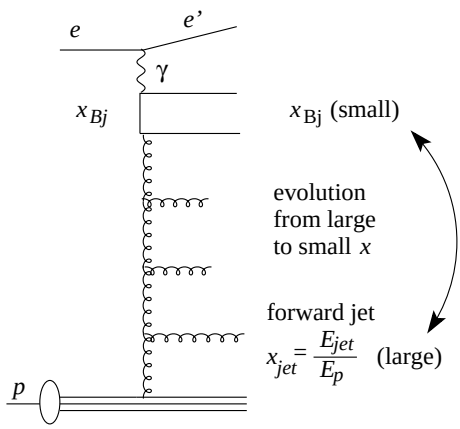

Fig. 6. Schematic view of a parton cascade leading to forward jet production at low x.

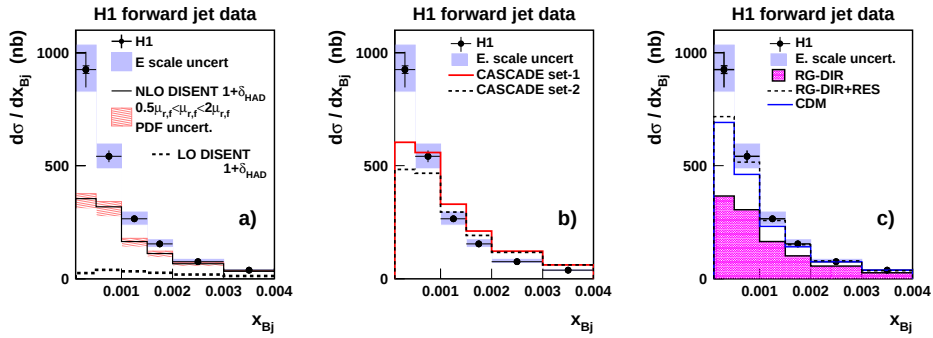

Fig. 7. Hadron level cross sections for forward jet production as a function of x_{Bj} compared to NLO predictions from DISENT (a) and to QCD Monte Carlo models (b and c) [6].

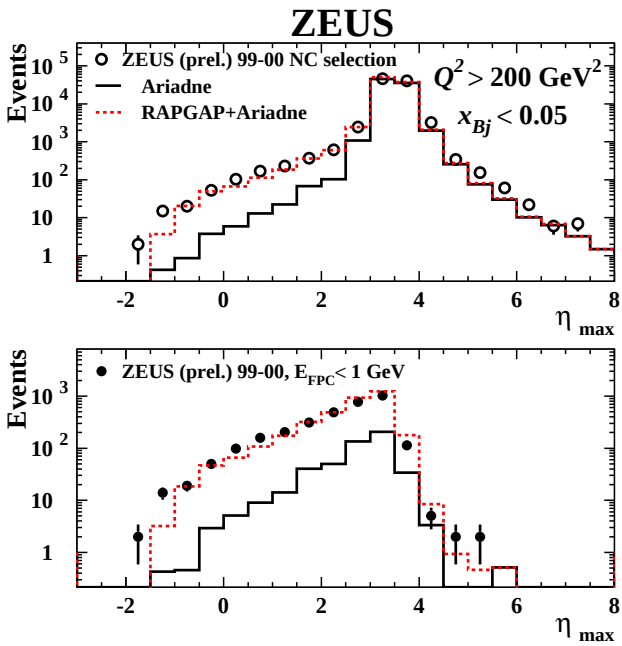

Fig. 8. Distribution of η_{max} for NC DIS events. The circles are the data-points, the solid line shows the result of the non-diffractive simulation (ARIADNE), the dashed line includes in addition the diffractive (RAPGAP) MC sample (top). In the bottom plot, an additional proton remnant veto using the energy measured in the forward plug calorimeter (FPC) has been applied.

characterized by a rapidity gap next to the outgoing proton, which is caused by the colorless exchange. The experimental measure characterizing the rapidity gap size is η^{max}, which is the pseudo-rapidity of the calorimeter energy deposit closest to the proton beam direction. Low values of η^{max} are indicative of a large rapidity gap. The measured distribution of neutral current events for $Q^2 > 200\ GeV^2$ is shown in fig. 8 [8]. In the region $\eta^{max} < 3$, an excess of events above the (non-diffractive) expectation of the ARIADNE model is clearly seen in the upper plot. The selection of rapidity gap events can be further purified by using the energy measured in ZEUS forward plug calorimeter (FPC), which extends the forward calorimeter coverage of the ZEUS uranium calorimeter by about one unit, as a veto against non-diffractive events with a very narrow proton remnant, as shown in the bottom part of fig. 8.

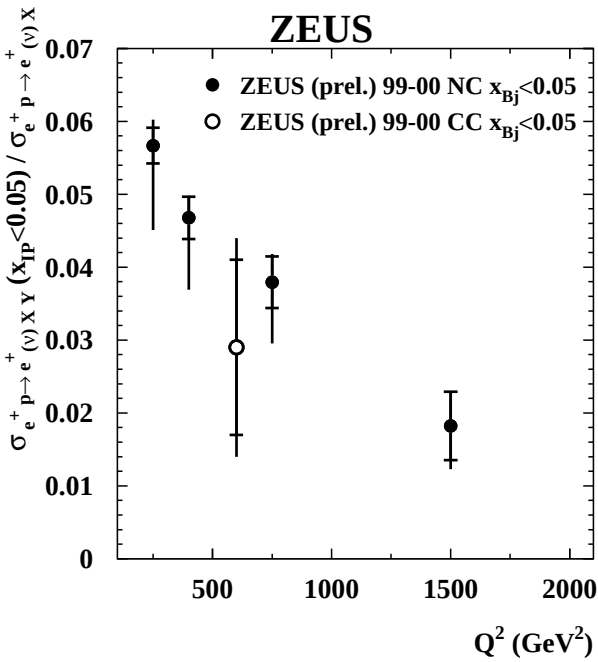

Fig. 9. Ratio of large rapidity cross section to the total cross section for both NC and CC interactions.

The result is presented as the ratio of the large rapidity gap cross section to the total cross section in fig. 9 for both neutral current (NC) and charged current (CC) production, as a function of Q^2 for $Q^2 > 200\ GeV^2$. For NC interactions, the diffractive contribution decreases from about 6% to 2% at $Q^2 = 1500\ GeV^2$, which indicates the persistence of diffractive interactions even at very hard scales. The

fraction for CC production is comparable to that for NC interactions, which shows that the probability of diffractive excitation of the photon is similar to that of the W boson.

5 Muons from Heavy Flavor Decays

One of the sources contributing to muon rates are decays of heavy flavors, which play a particularly important rôle at high transverse momentum. Several probes are commonly used to tag heavy quark production, for example decay impact parameter, or lepton transverse momentum relative to the jet. In the following, a di-muon signature will be discussed, which exploits the correlation between two muons from beauty decays [9]. This permits to use relatively low p_T thresholds for the individual muons, and allows measuring of the total $b\bar{b}$ cross section.

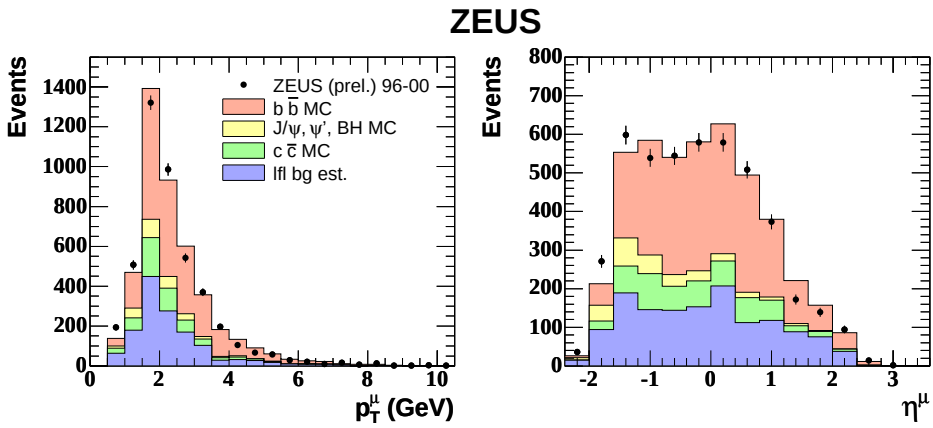

Fig. 10. Muon transverse momentum (left) and pseudorapidity distributions (right) in the non-isolated unlike-sign di-muon sample, together with the breakdown of expected contributions.

The signal stems from muonic semi-leptonic decays of a pair of B hadrons, which give rise to two oppositely charged muons, unless one of the B hadrons (B^0 or B_s) underwent oscillation into its anti-particle prior to decay. These muons tend to be in different hemispheres, with a large combined invariant mass. The main backgrounds come from charm pair production, heavy quarkonia and Bethe-Heitler processes. The charm production background is normalized to the charm contribution of a simultaneously measured $D^*\mu$ sample which has a very similar topology. Heavy quarkonia and Bethe-Heitler contributions lead mostly to isolated muons, and are reduced by applying a non-isolation requirement. Also light flavors contribute via semi-leptonic kaon or pion decays or hadron misidentification, in which case the charges are almost uncorrelated, so that the difference between unlike-sign and same-sign signals is essentially free of fake-muon backgrounds. The beauty signal

is therefore extracted from this difference, while the like-sign sample is used to fix the contribution of fake muon background to the unlike-sign sample.

Figure 10 shows the muon p_T and η distributions for non-isolated unlike-sign dimuon pairs, with the different contributions overlaid as described by the Monte Carlo with the normalizations derived as described. A total beauty content of about 1800 events is obtained with a purity of about 50%.

The low p_T threshold and large pseudo-rapidity coverage allow extraction of the total beauty cross section, which is determined as

$$\sigma_{tot}(ep \to b\bar{b}X) = 16.1 \pm 1.8(stat.)^{+5.3}_{-4.8}\ (syst.)nb$$

This result is compared to next-to-leading-order QCD calculations by adding the predictions of FMNR[10] and HVQDIS[11] with the CTEQ5M/CTEQ5F4 structure functions. The resulting cross section of

$$\sigma^{NLO}_{tot}(ep \to b\bar{b}X) = 6.8^{+3.0}_{-1.7}\ nb$$

is by a factor of 2.4 lower than the measured value, though still compatible within uncertainties.

It is instructive to compare this result with a recent measurement of the visible $b\bar{b}$ cross section in photo-production using $D^*\mu$ correlations [12]. The results are shown in table 1 and in comparison to theory they display a similar trend.[1])

	Cross section [pb]	Data/Theory
Data	$206 \pm 53 \pm 35$	
PYTHIA (direct)	57 (44)	3.6
CASCADE	56	3.7
FMNR	$52\ ^{+14}_{-9}$	4.0

Table 1. Visible $b\bar{b}$ photoproduction cross section in the $D^*\mu$ as measured by the H1 experiment [12], in comparison to theory. The kinematic region is defined by $p_T(D^*) > 1.5\ GeV$, $|\eta(D^*)| < 1.5$, $p(\mu) > 2\ GeV$, $|\eta(\mu)| < 1.735$, $0.05 < y < 0.75$ and $Q^2 < 1\ GeV^2$.

6 Summary

The colliding beam experiments H1 and ZEUS provide a wealth of measurements of the hadronic final state at HERA. Accurate determinations of leading baryon and forward jet production challenge the present models, and provide a concise experimental basis for an improved theoretical understanding of the proton remnant hadronization area. Diffractive final states with large rapidity gaps are found to contribute to the DIS cross section at Q^2 ranges as high as 1500 GeV^2.

[1]) The absolute numbers cannot be compared directly to the di-muon results because they refer to a restricted kinematical area.

Di-muon and $D^*\mu$ correlations allow study of the total beauty production cross section, which appears to be in excess of the NLO QCD calculations.

References

[1] H1 Collaboration, http://www-h1.desy.de/h1/www/pictures/list.html.

[2] G. Bruni, G. Iacobucci and L. Rinaldi, *Study of DIS events containing a leading proton in ep collisions at HERA*, HERA-LHC Workshop Meeting, CERN, Geneva, March 2004.

[3] ZEUS Collaboration, *Study of DIS events containing a leading proton in e^+p collisions at HERA*, Int. Europhysics Conference on High Energy Physics, Aachen 2003.

[4] ZEUS Collaboration, *Leading neutron p_T distributions in deep inelastic scattering and photoproduction at HERA*, Symp. on Lepton-Photon Interactions at High Energy, Uppsala 2005.

[5] H1 Collaboration (A. Aktas et al.), Eur. Phys. J.C41:273-286, 2005.

[6] H1 Collaboration (A. Aktas et al.), *Forward jet production in deep inelastic scattering at HERA*, arXiv:hep-ex/0508055.

[7] Please see comprehensive literature referenced in [6].

[8] ZEUS Collaboration, *Observation of large rapidity gap events in charged and neutral current high Q^2 DIS at HERA*, Int. Symp. on Lepton-Photon Interactions at High Energy, Uppsala 2005.

[9] ZEUS Collaboration, *Measurement of beauty production from dimuon events at HERA*, Int. Symp. on Lepton-Photon Interactions at High Energy, Uppsala 2005.

[10] S. Frixione, P. Nason and G. Ridolfi, Nucl. Phys. B454, 3 (1995).

[11] B.W. Harris and J. Smith, Nucl. Phys. B452, 109 (1995);
B.W. Harris and J. Smith, Phys. Lett. B353, 535 (1995). Erratum-ibid B359, 423 (1995).

[12] H1 Collaboration (A. Aktas *et al.*), Phys. Lett. B **621**, 56 (2005).